
XOOD: Extreme Value Based Out-Of-Distribution Detection For Image Classification

Frej Berglind

Louisiana State University
Baton Rouge, LA 70803
fberg11@lsu.edu

Haron Temam

Louisiana State University
Baton Rouge, LA 70803

Supratik Mukhopadhyay

Louisiana State University
Baton Rouge, LA 70803

Kamalika Das

Intuit Inc.
2700 Coast Ave
Mountain View CA 94043

Md Saiful Islam Sajol

Louisiana State University
Baton Rouge, LA 70803

Sricharan Kumar

Intuit Inc.
2700 Coast Ave
Mountain View CA 94043

Kumar Kallurupalli

Intuit Inc.
2700 Coast Ave
Mountain View CA 94043

Abstract

Detecting out-of-distribution (OOD) data at inference time is crucial for many applications of machine learning. We present XOOD: a novel extreme value-based OOD detection framework for image classification that consists of two algorithms. The first, XOOD-M, is completely unsupervised, while the second XOOD-L is self-supervised. Both algorithms rely on the signals captured by the extreme values of the data in the activation layers of the neural network in order to distinguish between in-distribution and OOD instances. We show experimentally that both XOOD-M and XOOD-L outperform state-of-the-art OOD detection methods on many benchmark data sets in both efficiency and accuracy, reducing false-positive rate (FPR95) by 50%, while improving the inferencing time by an order of magnitude.

1 Introduction

Deep neural networks are known to be opaque in their decision-making process [1]. This becomes problematic when decisions need to be made on inputs whose salient characteristics are different than what the neural network has been trained to identify. Such situations frequently arise when dealing with out-of-distribution (OOD) data [2], i.e., test data at inference time that does not come from the training distribution. For example, a neural network that has been trained to classify images of horses and giraffes, when provided with an image of an elephant, will classify it either as a horse or a giraffe, rather than determining that it does not belong to either of the classes. Indeed, the fundamental assumption in supervised machine learning that both the training and the test data come from the same probability distribution [3, 4], is violated in many real-world applications like text extraction from documents, medical diagnosis, autonomous driving, etc. In such situations, neural networks can make erroneous decisions rather than issuing a warning that they have encountered OOD data on which their decisions cannot be trusted. When document text extraction models are deployed in real life applications, they may encounter a crumpled document that is damaged beyond recognition. Instead of informing the users of the situation, the model will attempt to extract a (possibly incorrect) set of texts from it. In safety critical decision making such as medicine, finance, and autonomous

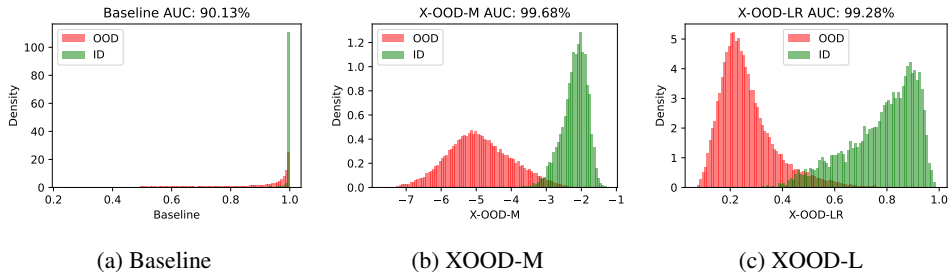


Figure 1: Comparison of the baseline result from the softmax output of a ResNet34 to our out-of-distribution detection algorithms. In this example, cifar-10 is in-distribution (ID) and SVHN is out-of-distribution (OOD). Note how confident the baseline is even though the images in SVHN do not belong to any of the classes in cifar-10.

driving, for machine learning models to be trusted, it is important for the model to identify when to abstain or require human intervention [5].

It is well known [6, 7] that the “class probabilities” output by the softmax layer of a neural network are only weakly correlated with how confident the model should be about the prediction, even in the relatively simple case of distinguishing Gaussian noise from in-distribution data [6]. Measuring uncertainty associated with the decisions of a neural network during inference time is an active area of research [8]. For uncertainties stemming from encountering OOD data at test time, various supervised and unsupervised methods have been proposed in the literature [9], [10], [11], [12] that provide varying degree of accuracy and come with varying degrees of computational overhead. Since convolutional layers have linear complexity, OOD detection algorithms for convolutional networks should ideally have linear complexity in order to be useful and scalable in real life applications. In this paper, we propose a class of extreme value based OOD detection algorithms that are linear in complexity with respect to the size of the embedding space, and are, therefore, highly efficient and scalable, while matching or beating state of the art results in accuracy metrics.

Our XOOD framework (Extreme Value-based OOD Detection) that comprises two efficient and accurate algorithms for OOD detection *for image classification*: the first, XOOD-M, being completely unsupervised (see Section 2.2.2), while the second XOOD-L being self-supervised (see Section 2.2.3). Neither of the two algorithms require prior knowledge of the OOD data, but instead rely on the computation of global extrema of the input features. Figure 1a presents the softmax output of a ResNet34 with CIFAR-10 as in-distribution and SVHN as OOD. As one can see, the softmax output is unable to separate between the in-distribution and the OOD images. Figures 1b and 1c respectively show that both the unsupervised as well as the self-supervised algorithms of XOOD (XOOD-M and XOOD-L) are able to separate the in-distribution from the OOD images. In addition, both algorithms are robust to both uniform and Gaussian noise (see Table 5 in Appendix A).

Contributions: This paper makes the following contributions

- Based on the observation that the extreme value distribution of the feature space in any activation layer is unimodal on the in-distribution data, we propose a highly effective method for OOD detection using these extrema.
- We introduce a regularized Mahalanobis distance on the extracted extreme values for unsupervised OOD detection (XOOD-M).
- We present a self-supervised method using logistic regression on the extracted extreme values for OOD detection (XOOD-L).
- We show experimentally that both XOOD-M and XOOD-L outperform state-of-the-art OOD detection methods on many benchmark data sets across several detection metrics. In fact, it improves the average false positive rate at 95% true positive rate by as much as 50% compared to the best performing existing approach [9].
- Both algorithms have an order-of-magnitude lower computational overhead compared to several other state-of-the-art OOD detection methods and scale linearly with the size of the embedding space, making them ideal for many real-life applications.

2 Proposed Approach

In this section, we formally define the problem statement, and discuss the theoretical background of our proposed methods before describing the two algorithms for OOD detection.

2.1 Problem Formulation

A neural network based image classifier is a function $f_\theta : X \rightarrow Y$, where θ represents the weights of the network, X is the input domain defined by a set of images and $Y = \{0, 1, \dots, K - 1\}$, where K is the number of classes in the input distribution. In the traditional image classification setting, the trained model f_θ outputs a decision $\hat{y} \in Y$ for every test image \tilde{X} . However, if \tilde{X} is out of distribution with respect to the input distribution of X , we would want the model f_θ to return, along with the class label \hat{y} , a score akin to model confidence that can indicate whether \tilde{X} is out of distribution with respect to the marginal probability distribution p_X for the joint distribution $p(X, Y)$. In other words, we want to learn a function g that satisfies the following condition

$$g(\tilde{X}) = \begin{cases} 1 & \text{if } \tilde{X} \sim p_X \\ 0 & \text{otherwise} \end{cases} \quad (1)$$

2.2 Extreme Value Based Out-Of-Distribution Detection

We propose two new extreme value based out-of-distribution detection algorithms that rely on the signals captured by the extreme values of the data in the activation layers of a neural network to distinguish between in distribution and OOD instances. Neither of the two algorithms require prior knowledge of the OOD data. The first algorithm, called XOOD-M, is completely unsupervised. It only computes some statistics on the extreme value distribution of the training data and uses the notion of distance from those statistics to identify OOD data points. This method is extremely efficient and accurate and produces state-of-the-art results on all benchmark data sets for which the extreme value distribution of the training data is compact and well separated from the OOD data. For situations where the OOD data may not be significantly different than the in-distribution data, we propose a modified version of the XOOD-M algorithm called XOOD-L. This is a self-supervised algorithm in that it does not need to be trained on labeled OOD detection data. Instead, it learns a logistic regression model on the extreme values of the in-distribution data along with a range of distortions of that data as a surrogate for the OOD data. XOOD-L also beats state-of-the-art OOD detection methods on many benchmark data sets in both efficiency and accuracy.

We describe the details of both the algorithms in the next few sections.

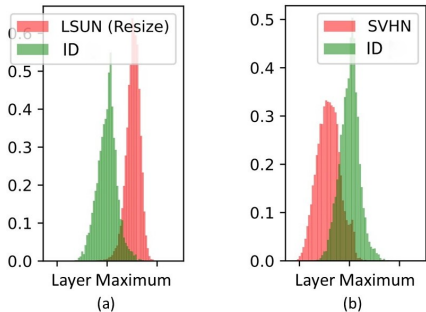


Figure 2: Distribution of maximum values before an activation layer inside ResNet34. Green represents CIFAR-10 (ID) and Red represents LSUN-Resize(OOD) (left figure) or SVHN(OOD) (right figure). Note how in-distribution data lies in a single mode, while out-of-distribution data can be on either side. Complete examples of extreme values can be found in Appendix C

2.2.1 Extreme Value Extraction

The essence of both the algorithms is in the nature of the distribution of the extreme values of the data as it enters the activation layers in a neural network. We observe that the per activation layer

distribution of maximum or minimum value is consistently unimodal on in-distribution data, as can be seen in Figure 2 and Appendix C. Based on this observation, we compute the global maximum and minimum of the input images before each activation layer in the architecture. To improve the symmetry of this distribution, we apply a Yeo-Johnson transform [13] fitted on the extreme values of the training data. The output of this transform is standardized to zero mean and unit variance. This computation does not make use of class labels or image topology, yet it is highly effective for OOD detection.

Function: ExtremeValueExtraction

Require: Data set X_t
for each image $X_{t,i}$ in training set X_t **do**
 $X_{min,i}, X_{max,i} = \text{MinMax}(X_{t,i})$
end for
 $X_{min} = [X_{min,1}, X_{min,2}, X_{min,3}, X_{min,4}, \dots]$
 $X_{max} = [X_{max,1}, X_{max,2}, X_{max,3}, X_{max,4}, \dots]$
return X_{min}, X_{max}

2.2.2 Unsupervised Out-of-Distribution Detection: XOOD-M

Once the extreme values are computed for each activation layer of the neural network, a regularized Mahalanobis distance can be used for OOD detection. Let μ and M be the mean and covariance of the extreme values on the training set. We modify M by adding a constant to the diagonal:

$$M' = M + C \cdot I, \quad (1)$$

where $C \in [0, \text{inf})$ is a regularization constant and I is the identity matrix. Since the extreme values are standardized, the diagonal of M is 1 and we can expect C to have a consistent effect on each instance. The Mahalanobis distance D_M is computed using

$$D_M(x) = \sqrt{(x - \mu)^\top (M + C \cdot I)^{-1} (x - \mu)}. \quad (1)$$

The value $C = 0$, corresponds to the standard Mahalanobis distance, that represents the likelihood of a multivariate normal distribution. If C is large, the regularized covariance matrix M' and the corresponding inverse covariance matrix $(M')^{-1}$ are dominated by the constant on the diagonal and D_M is approximately proportional to the L^2 distance. This corresponds to the likelihood of a normal distribution where each of the extreme values are independent. The regularizer C allows us to control the definition of in-distribution data. Algorithm 1 presents the pseudo-code of the XOOD-M algorithm. As can be seen from the pseudo-code, XOOD-M has minimal computational overhead. The only features that are computed on the training data are mean and covariance on the extreme value feature set, which is low dimensional with only $2 \times r$ features, where r is the number of activation layers in the network.

Algorithm 1: XOOD-M

Require: Training image and label set $\langle X_t, y_t \rangle$, Pretrained classifier f_θ , Regularization C
Ensure: Mean μ and Covariance K of OOD features
 Predict $\hat{y}_t = f_\theta(X_t)$
 $X_t = X_{t, \hat{y}_t = y_t}$
 for each input $X'_{t,j}$ to activation layer j in f_θ **do**
 $X_{min,j}, X_{max,j} = \text{FeatureExtraction}(X'_{t,j})$
 $X_j^P, T_j^P = \text{fit.PowerTransform}(X_{min,j}, X_{max,j})$
 end for
 $\mu = \text{Mean}(X_j^P)$
 $M = \text{Covariance}(X_j^P)$

2.2.3 Self-supervised Out-of-Distribution Detection: XOOD-L

The extreme value feature set extracted from the training data can be used in a self-supervised setting for OOD detection. While the Mahalanobis distance-based method produces a set of distances from

the in-distribution features, using a logistic regression-based method it is possible to generate labels to classify points as out of OOD, as shown in Equation 1. Additionally, the calibrated probability scores of the logistic regression model can directly be interpreted as the amount of confidence of the model based on the similarity of the test instance with instances seen during training. The logistic regression model predicts the likelihood of an instance being in-distribution based on the distribution of the extreme values in each activation layer. It uses the extreme value features obtained from the training data as well as *distorted* calibration data (see Section 2.2.4) for training the model. The labels of the instances are generated based on whether the pre-trained neural network model can correctly predict each instance or not: all correctly classified instances are assigned label 1 in the logistic regression training, while all incorrectly classified instances have label 0. The intuition behind this is that, OOD data should be further away from the in-distribution data than images where the model makes a meaningful prediction. Therefore, this logistic regression should generalize to OOD images and assign them predictions close to 0. As shown in Figure 2, sometimes the distorted data is mapped to both sides of the in-distribution mode of the extreme value distribution. To enable the logistic regression to handle this, we split up the extreme values for each layer around the mean of the in-distribution data:

$$\begin{cases} m_i^+ = \text{relu}(m_i - \bar{m}_i) \\ m_i^- = \text{relu}(-m_i + \bar{m}_i) \end{cases} \quad (1)$$

where m_i is maximum or minimum for activation layer i and \bar{m}_i is the mean of on the in-distribution data. Lastly, before applying the logistic regression, each of the split up extreme values are scaled to zero mean and unit variance to ensure consistent regularization. To avoid overfitting to the logistic regression training data, we apply ℓ_2 -regularization which is tuned through k-fold cross validation where each fold excludes one of the distortion types. Algorithm 2 describes the pseudo-code of the XOOD-L algorithm.

Algorithm 2: XOOD-L

Require: Training image and label set $\langle X_t, y_t \rangle$, Calibration image and label set $\langle X_c, y_c \rangle$,
Require: Number of distortions to be applied k , Distortion parameters d , Pretrained classifier f_θ
Ensure: Logistic regression model $g(w, \lambda)$ for training module

```

Predict  $\hat{y}_t = f_\theta(X_t)$ 
 $X_t = X_{t, \hat{y}_t = y_t}$ 
for each input  $X'_{t,j}$  to activation layer  $j$  in  $f_\theta$  do
     $X_{min,j}, X_{max,j} = \text{FeatureExtraction}(X'_{t,j})$ 
     $X_j^P, T_j^P = \text{fit.PowerTransform}(X_{min,j}, X_{max,j})$ 
end for
for  $i \in 1, \dots, k$  do
     $X_{D_i} = \text{Distortion}(X_c, d_i)$ 
end for
 $Z = [X_C, X_{D_1}, X_{D_2}, \dots, X_{D_k}]$ 
for each input  $Z'_j$  to activation layer  $j$  in  $f_\theta$  do
     $Z_{min,j}, Z_{max,j} = \text{ExtremeValueExtraction}(Z'_j)$ 
     $Z_j^P = T_j^P.\text{PowerTransform}(Z_{min,j}, Z_{max,j})$ 
end for
Predict  $\hat{y}_c = f_\theta(Z)$ 
 $LR_x = [Z_{min,1} Z_{max,1} Z_{min,2} Z_{max,2} Z_{min,3} Z_{max,3} \dots]$ 
if  $\hat{y}_c == y_c$  then
     $LR_y = 1$ 
else
     $LR_y = 0$ 
end if
 $\lambda = \text{crossValidate.LogisticRegression}(LR_x, LR_y)$  using each distorted data subset  $X_{D_i}$ 
and  $X_C$  as validation set to a  $(k + 1)$ -fold cross validation
 $w = \text{fit.LogisticRegression}(LR_x, LR_y, \lambda)$ 

```

2.2.4 Design Choices in Models

In both XOOD-M and XOOD-L, we make various choices in terms of the feature set, the distortions, and the regularization. In this section we discuss the rationale behind these choices.

Distortions The distortions were designed to create a wide range of colors and textures, challenge the classifier in many different ways and produce wide and smooth distributions of extreme values. For satisfying these requirements, we used the following distortions in XOOD-L:

1. **Geometric:** A combination of common geometric image augmentations: up to 90 degree rotation, up to 0.2 width and height shift, 50% chance of horizontal flip, brightness range between 0.2 and 2, zoom range from 0.9 to 1.1.
2. **Mixup:** A convex combination of two images in the data set. The label is taken from the image with the highest weight. This produces images with less distinct features which lie near a decision boundary.
3. **Gaussian Noise:** Additive Gaussian noise with mean 0 and variance ranging from 0 to 2. After adding noise we apply an affine transformation to each pixel value to create a wide range of brightness and contrast $x = ax + b$, where $a \in [1/8, 8]$ and $b \in [\min(0, 1 - a), \max(0, 1 - a)]$. a and b are constant for every image.
4. **Gaussian Blur:** Gaussian blur with mean 0 and variance ranging from 0.2 to 5. After blurring the images we apply the same affine transformation as for the Gaussian noise.

All resulting images are clipped to have pixel values between 0 and 1.

Regularization While the ℓ_2 regularization in the XOOD-L method is tuned through cross validation, the regularization parameter C in XOOD-M cannot be learnt. So we experimented with a wide range of values for C . We found that a regularization $C = 10$ worked well across all architectures and data sets. Figure 3 shows a comparison of detection performance with C ranging from 0 to ∞ , where ∞ corresponds to L_2 -distance instead of Mahalanobis distance.

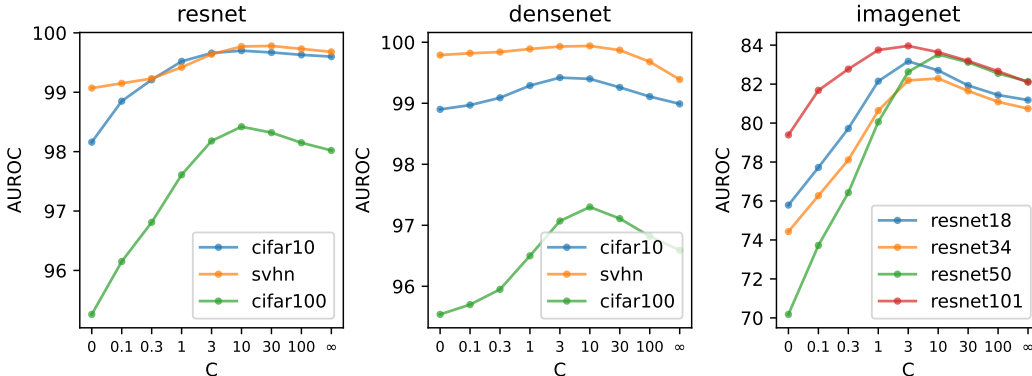


Figure 3: AUROC-score of XOOD-M for various regularization values. The score was computed on the test set and the union of TinyImageNet (Crop), TinyImageNet (Resize), LSUN (Crop), LSUN (Resize), iSUN for CIFAR-10, CIFAR-100 and SVHN. For CIFAR-10 and CIFAR-100, SVHN is included as OOD as well. For IMAGENET-1000, we used Places, SUN, iNaturalist and DTD, as curated by [12].

Feature Set Although we based our algorithm on the extreme value distribution of the data in the activation layers, we experimented with a number of different features: only using the minimum or maximum, the sum; the percentage of positive values; L_p -norms; L_p -norms of $ReLU(x)$ and $ReLU(-x)$. As one can see in Appendix B, neither replacing the extreme values by these features, nor adding these features while still using the extreme values improves the detection performance.

3 Experiments

In this section, we report the results obtained from running XOOD-M and XOOD-L on a variety of data sets on a number of performance metrics. The code is available at [14]. We track performance with respect to the quality of the results as well as the efficiency of the methods. For quality of results, we measure performance based on the following metrics:

- **AUROC:** The area under plot of true positive rate (TPR) versus false positive rate (FPR). A random detector has AUROC = 50% and an ideal detector has AUROC = 100%.
- **TNR (95% TPR):** The probability that an OOD instance is correctly detected with a threshold that achieves a TPR of 95%.
- **Detection Accuracy:** The maximum detection accuracy over all thresholds, assuming equal amounts of in-distribution and OOD instances. That is, $\max_T \left\{ \frac{p(f(x) > T | x \in \text{ID}) + p(f(x) \leq T | x \in \text{OOD})}{2} \right\}$, where f is the confidence score.

3.1 Results

We have tested the XOOD algorithms on ResNet and DenseNet for Cifar-10, Cifar-100, and SVHN using the same pretrained models as several other papers on OOD-detection. In Tables 2 and 1, we compare our algorithms with the baseline [6], ODIN [10], Mahalanobis [15] and Gram [9]. Even though ODIN and Mahalanobis are trained on a sample of the OOD-data, XOOD outperforms them in most cases. And even though Gram is far more computationally complex, XOOD outperforms it in most experiments. The one case where XOOD struggles is CIFAR-100 vs CIFAR-10. However, this is not necessarily bad, because the datasets are very similar. For example, CIFAR-10 includes cars, trucks and dogs, while CIFAR-100 contains pickup trucks, busses and wolfs. If all of these are detected as OOD, it limits the generalization ability of the model.

Table 1: **DenseNet** detection scores for Baseline/Odin/Mahalanobis/Gram/XOOD-L/XOOD-M. Results for other algorithms are from Sastry and Oore [16].

In Dist	Out Dist	TNR (95% TPR)	AUROC	Detection Acc.
CIFAR-10	CIFAR-100	40.3/ 53.1 /14.5/26.7/47.6/19.9	89.3/ 90.2 /58.5/72.0/87.0/70.7	82.9 /82.7/57.2/67.3/78.6/64.8
	LSUN-C	51.8/70.6/48.2/88.4/ 96.9 /91.7	92.9/93.6/80.2/97.5/ 99.3 /98.4	86.9/86.4/75.6/92.0/ 96.1 /93.6
	LSUN-R	66.6/96.2/97.2/99.5/99.4/ 99.7	95.4/99.2/99.3/ 99.9 / 99.9 / 99.9	90.3/95.7/96.3/ 98.6 /98.5/ 98.6
	SVHN	40.2/86.2/90.8/96.1/96.5/ 97.2	89.9/95.5/98.1/99.1/99.2/ 99.3	83.2/91.4/93.9/95.9/96.2/ 96.7
	TinyImgNet-C	56.7/87.0/84.2/96.7/ 98.6 /97.8	93.8/97.6/95.3/99.3/99.7/99.5	88.1/92.3/89.9/96.1/ 97.7 /96.6
	TinyImgNet-R	58.9/92.4/95.0/98.8/99.1/ 99.2	94.1/98.5/98.8/99.7/ 99.8 / 99.8	88.5/93.9/95.0/97.9/ 98.2 /97.8
	iSUN	62.5/93.2/95.3/99.0/ 99.5 /99.4	94.7/98.7/98.9/99.8/ 99.9 /99.8	89.2/94.3/95.2/97.9/ 98.5 /98.1
CIFAR-100	CIFAR-10	18.9 /16.8/ 7.7/10.6/10.0/ 1.7	75.9 /74.2/60.1/64.2/65.0/43.1	69.7 /68.6/57.8/60.4/61.8/50.0
	LSUN-C	28.6/57.8/42.1/65.5/ 84.9 /68.4	80.2/91.4/81.7/91.4/ 97.4 /92.6	72.7/83.3/74.0/83.6/ 91.3 /85.0
	LSUN-R	17.6/41.2/91.4/97.2/94.3/ 97.9	70.8/85.5/98.0/ 99.3 /99.0/ 99.3	64.9/77.1/93.9/96.4/94.8/ 96.7
	SVHN	26.7/70.6/82.5/ 89.3 /88.8/87.9	82.7/93.8/97.2/97.3/ 97.7 /97.1	75.6/86.6/91.5/ 92.4 /92.3/91.9
	TinyImgNet-C	24.6/51.0/60.1/89.0/ 95.4 /89.2	76.2/88.3/88.8/97.7/ 99.1 /97.5	69.0/80.2/81.6/92.5/ 95.2 /92.7
	TinyImgNet-R	17.6/42.6/86.6/95.7/95.7/ 96.1	71.7/85.2/97.4/99.0/ 99.2 /98.9	65.7/77.0/92.2/95.5/95.4/ 95.6
	iSUN	14.9/37.4/87.0/95.9/94.0/ 96.3	69.5/84.5/97.4/ 99.0 /98.9/ 99.0	63.8/76.4/92.4/95.6/94.6/ 95.7
SVHN	CIFAR-10	69.3/71.7/96.8/80.4/ 99.7 /98.4	91.9/91.4/98.9/95.5/ 99.8 /99.5	86.6/85.8/95.9/89.1/ 98.3 /97.0
	LSUN-R	77.1/81.1/99.9/99.5/ 100. / 100.	94.1/94.5/99.9/99.8/ 100. / 100.	89.1/89.2/99.3/98.6/ 99.8 / 99.8
	TinyImgNet-R	79.8/84.1/99.9/99.1/ 100. / 100.	94.8/95.1/99.9/99.7/ 100. / 100.	90.2/90.4/98.9/97.9/99.5/ 99.6
	iSUN	78.3/82.2/99.9/99.4/ 100. / 100.	94.4/94.7/99.9/99.8/ 100. / 100.	89.6/89.7/99.2/98.3/99.7/ 99.8

To summarize the performance of the various methods, we computed the mean scores across all metrics for each OOD detection task, except the CIFAR-10–CIFAR-100 in-distribution-OOO combination, given their overlap. We observe that XOOD-L and XOOD-M have the best FPR (95% TPR) across all architectures, beating the state-of-the-art Gram method by approximately 50%. For details, please refer to the Appendix D (Table 8).

3.2 Inference Time

In real-world applications of OOD-detection, the inference time is often crucial, yet this has largely been neglected in research. We measured the inference time of a ResNet and DenseNet on cifar10 and cifar100 for the baseline [6], Mahalanobis [15], Gram [9] and XOOD. We chose to compare with

Table 2: **ResNet34** detection scores for Baseline/Odin/Mahalanobis/Gram/XOOD-L/XOOD-M. Results for other algorithms are from Sastry and Oore [16].

In Dist	Out Dist	TNR (95% TPR)	AUROC	Detection Acc.
CIFAR-10	CIFAR-100	33.3/42.0/41.6/32.9/ 43.6 /32.0	86.4/85.8/88.2/79.0/ 88.8 /80.1	80.4/78.6/81.2/71.7/ 81.7 /73.7
	LSUN-C	48.6/62.0/81.3/89.8/ 97.0 /94.6	91.9/91.2/96.7/97.8/ 99.4 /99.0	86.3/82.4/90.5/92.6/ 96.0 /94.8
	LSUN-R	49.8/82.1/98.8/99.6/99.1/ 99.9	91.0/94.1/99.7/99.9/99.8/ 100.	85.3/86.7/97.7/98.6/97.8/ 99.2
	SVHN	50.5/70.3/87.8/97.6/96.4/ 98.4	89.9/96.7/99.1/99.5/99.3/ 99.7	85.1/91.1/95.8/96.7/96.1/ 97.6
	TinyImgNet-C	46.4/68.7/92.0/96.7/98.0/ 99.1	91.4/93.1/98.6/99.2/99.5/ 99.8	85.4/85.2/93.9/96.1/96.7/ 98.0
	TinyImgNet-R	41.0/67.9/97.1/98.7/97.9/ 99.5	91.0/94.0/99.5/99.7/99.6/ 99.9	85.1/86.5/96.3/97.8/96.9/ 98.8
CIFAR-100	iSUN	44.6/73.2/97.8/99.3/99.1/ 99.7	91.0/94.0/99.5/99.8/99.8/ 99.9	85.0/86.5/96.7/98.1/97.8/ 98.8
	CIFAR-10	19.1/18.7/ 20.2 /12.2/11.7/9.3	77.1/77.2/77.5/67.9/71.0/63.9	71.0/71.2/72.1/63.4/67.1/61.6
	LSUN-C	18.7/44.1/64.8/64.8/ 85.3 /76.2	75.5/82.7/92.0/92.1/ 97.5 /95.3	69.2/75.9/84.0/84.2/ 91.4 /88.2
	LSUN-R	18.8/23.2/90.9/96.6/90.2/ 98.5	75.8/85.6/98.2/99.2/98.3/ 99.6	69.9/78.3/93.5/96.7/92.9/ 97.4
	SVHN	20.3/62.7/91.9/80.8/87.2/ 92.1	79.5/93.9/ 98.4 /96.0/97.6/98.2	73.2/88.0/ 93.7 /89.6/91.5/93.6
	TinyImgNet-C	24.3/44.3/80.9/88.5/90.8/ 95.0	79.7/85.4/96.3/97.7/98.4/ 98.9	72.5/78.3/89.9/92.2/93.2/ 95.0
SVHN	TinyImgNet-R	20.4/36.1/90.9/94.8/89.4/ 97.9	77.2/87.6/98.2/98.9/98.1/ 99.5	70.8/80.1/93.3/95.0/92.6/ 96.7
	iSUN	16.9/45.2/89.9/94.8/89.6/ 97.0	75.8/85.5/97.9/98.8/98.3/ 99.3	70.1/78.5/93.1/95.6/92.8/ 96.2
	CIFAR-10	78.3/79.8/ 98.4 /85.8/98.1/96.1	92.9/92.1/99.3/97.3/ 99.5 /98.9	90.0/89.4/ 96.9 /92.0/96.8/95.7
	LSUN-R	74.3/77.3/ 99.9 /99.6/99.5/ 99.9	91.6/89.4/ 99.9 /99.8/ 99.9 /99.9	89.0/87.2/ 99.5 /98.5/98.3/98.9
	TinyImgNet-R	79.0/82.0/ 99.9 /99.3/99.7/99.8	93.5/92.0/ 99.9 /99.7/ 99.9 /99.8	90.4/89.4/ 99.1 /97.9/98.4/98.6
	iSUN	77.1/79.1/99.7/99.4/99.8/ 99.9	92.2/91.4/99.8/99.8/ 99.9 /99.9	89.7/89.2/98.3/98.1/98.7/ 98.9

Mahalanobis and Gram since they have good detection performance and use similar feature extraction schemes as XOOD. The results are shown in Tables 3 and 4. While XOOD has an overhead of about 30%, Mahalanobis and Gram impose more than a 10-fold increase in inference time. Mohseni et al. [17] compare the inference time of Outlier Exposure [18], Geometric OOD [19], shifting transformation learning [17], SSD [20], CSI [21], CSI-ens [21], and Gram [9]. All these algorithms have overhead above 100% except Outlier Exposure, which doesn't have any overhead at all, but it is not really comparable to XOOD since it requires fitting on OOD data.

The tables 2 and 1 display the time it takes to compute the classification and OOD detection of 10000 images consisting of Gaussian noise on a single *NVIDIA Tesla V100* GPU and one *Intel Xeon Silver 4216* CPU with a batch size of 128, averaged over 10 runs. We define overhead as $\frac{T-T_B}{T_B}$, where T is the average inference time and T_B is the average inference time of the baseline. Code for Mahalanobis [15] and Gram [9] was modified to enable this comparison. The computations in these algorithms do not depend on the content of the images and Gaussian noise was simply used for convenience.

Table 3: Average inference time measured in seconds of various OOD-detection algorithms on ResNet34. \pm indicates the 99%-confidence interval of the mean.

	(a) CIFAR-10		(b) CIFAR-100		
	Inference Time	Overhead	Inference Time	Overhead	
Baseline	1.45 \pm 0.0041	0%	Baseline	1.45 \pm 0.0069	0%
XOOD-L	1.79 \pm 0.0575	24%	XOOD-L	1.83 \pm 0.0913	26%
XOOD-M	1.99 \pm 0.0163	37%	XOOD-M	2.0 \pm 0.0177	38%
Mahalanobis	20.25 \pm 0.0413	1298%	Mahalanobis	28.02 \pm 0.4577	1834%
Gram	28.70 \pm 0.6036	1880%	Gram	28.49 \pm 0.1467	1866%

3.3 Further Experiments

Additionally, we compare the performance of XOOD with Energy [22] and ReAct [12] on DenseNet and ResNet34 for CIFAR-10, CIFAR-100 and SVHN, as well as ResNet18, ResNet34, ResNet50 and ResNet101 for Imagenet1000. A table with these results can be found in Appendix A. XOOD outperforms the other algorithms on CIFAR-10, CIFAR-100 and SVHN. ReAct performs the best on Imagenet1000, but does not significantly improve over the baseline on the other data sets. It also struggles with the Gaussian noise data set on Imagenet1000 and gets 0% TPR at 95% TNR for ResNet34 and ResNet50. XOOD-L outperforms the baseline and Energy on almost all combinations in in-distribution and OOD data sets.

Table 4: Average inference time measured in seconds of various OOD-detection algorithms on DenseNet. \pm indicates the 99%-confidence interval of the mean.

(a) CIFAR-10			(b) CIFAR-100		
	Inference Time	Overhead		Inference Time	Overhead
Baseline	2.24 ± 0.0102	0%	Baseline	2.23 ± 0.0056	0%
XOOD-L	2.90 ± 0.0497	29%	XOOD-L	2.91 ± 0.0849	31%
XOOD-M	3.12 ± 0.0480	39%	XOOD-M	3.08 ± 0.0188	39%
Mahalanobis	30.11 ± 0.2802	1246%	Mahalanobis	36.88 ± 0.6617	1557%
Gram	63.01 ± 0.7629	2717%	Gram	61.46 ± 0.6788	2662%

4 Related Work

The last few years have seen a tremendous amount of work in OOD detection [2, 10, 9, 12, 23, 10, 15, 23, 11, 22, 24, 25, 26, 27, 28, 29, 30]. However, as argued in [31], no single algorithm can be considered the state-of-the-art. In [31], the authors tested the algorithms in [10, 6, 15] on three benchmark in-distribution datasets (CIFAR-10, CIFAR-100, SVHN) and seven benchmark OOD datasets under standardized conditions. They found inconsistent performance of these algorithms across all the datasets; in fact, there was no algorithm that was consistently outperforming others across all the datasets. As shown in Tables 1, 2, for DenseNet and ResNet34 architectures, both XOOD-L and XOOD-M outperform [10, 6, 15] for CIFAR-10 (with LSUN-C, LSUN-R, SVHN, TinyImageNet-C, TinyImageNet-R, and iSun as OOD). Similar is the case with most other in-distribution-OOD combinations. Unlike algorithms like [10, 15, 22], neither XOOD-M nor XOOD-L require access to the OOD data during training time. In addition, for the architectures considered, both XOOD-L and XOOD-M outperform [9] for almost all in-distribution-OOD combinations. Mohseni et al. [17] compare different OOD detection algorithms in terms of inference time. All the algorithms considered, that are not allowed to train on OOD data, have overhead above 100%. Both the algorithms in [9, 15] involve matrix multiplication which has at least quadratic complexity. Since, the number of features within a neural network is large, matrix multiplication operations as used in [9, 15] are prohibitively expensive. In case of XOOD-M, Mahalanobis distance is computed on the extreme values which has dimension twice the depth of the model (typically at most 1000); hence Mahalanobis distance can be computed efficiently. This explains why both our algorithms XOOD-L and XOOD-M outperform [9] and [15] in terms of inference time by an order of magnitude. In Table 5 in Appendix A, we show that ReAct [12] is having difficulty distinguishing Gaussian noise from in-distribution ImageNet (Resnet 34 and ResNet 50). Table 5 also shows that both XOOD-L and XOOD-M are robust to Gaussian and uniform noise. Additionally, Table 5 shows that the XOOD framework (in particular XOOD-L) outperforms [22] on all but one (in-distribution CIFAR-10, OOD CIFAR-100) in-distribution-OOD data set combinations for all the architectures considered. ReAct performs the best on Imagenet1000, but does not significantly improve over the baseline on the other data sets.

5 Conclusions

We presented the XOOD framework (Extreme Value-based OOD Detection) that comprises two new, efficient and accurate algorithms for OOD detection for the image classification: the unsupervised XOOD-M, and the self-supervised XOOD-L. They rely on the signals captured by the extreme values of the data in the activation layers of the neural network to distinguish between in distribution and out of distribution instances. On most benchmark in-distribution-OOD dataset combinations, both XOOD-L and XOOD-M outperform state-of-the-art algorithms for standard architectures.

6 Limitations of the Work

The current work is focused on image classification. In future, we would like to extend the work to language models as well as graph neural networks, as well as test the XOOD algorithms in a more general confidence and calibration context.

7 Impact

When encountered with OOD examples at inference time, neural networks can make erroneous decisions rather than issuing a warning that their decisions in these cases cannot be trusted. Such behavior prevents their deployment in mission-critical application. The XOOD framework can help improve the trustworthiness of deep neural networks through efficient and accurate OOD detection. We do not anticipate any negative social consequences of our work.

References

- [1] Jeya Vikranth Jeyakumar, Joseph Noor, Yu-Hsi Cheng, Luis Garcia, and Mani Srivastava. How can i explain this to you? an empirical study of deep neural network explanation methods. *Advances in Neural Information Processing Systems*, 33:4211–4222, 2020.
- [2] Jingkang Yang, Kaiyang Zhou, Yixuan Li, and Ziwei Liu. Generalized out-of-distribution detection: A survey. *arXiv preprint arXiv:2110.11334*, 2021.
- [3] Christopher M Bishop et al. *Neural networks for pattern recognition*. Oxford university press, 1995.
- [4] Christopher M Bishop and Nasser M Nasrabadi. *Pattern recognition and machine learning*, volume 4. Springer, 2006.
- [5] David Gunning, Mark Stefik, Jaesik Choi, Timothy Miller, Simone Stumpf, and Guang-Zhong Yang. Xai—explainable artificial intelligence. *Science Robotics*, 4(37):eaay7120, 2019.
- [6] Dan Hendrycks and Kevin Gimpel. A baseline for detecting misclassified and out-of-distribution examples in neural networks. In *5th International Conference on Learning Representations, ICLR 2017, Toulon, France, April 24-26, 2017, Conference Track Proceedings*. OpenReview.net, 2017.
- [7] Anh Mai Nguyen, Jason Yosinski, and Jeff Clune. Deep neural networks are easily fooled: High confidence predictions for unrecognizable images. In *IEEE Conference on Computer Vision and Pattern Recognition, CVPR 2015, Boston, MA, USA, June 7-12, 2015*, pages 427–436. IEEE Computer Society, 2015.
- [8] Yaniv Ovadia, Emily Fertig, Jie Ren, Zachary Nado, David Sculley, Sebastian Nowozin, Joshua Dillon, Balaji Lakshminarayanan, and Jasper Snoek. Can you trust your model’s uncertainty? evaluating predictive uncertainty under dataset shift. *Advances in neural information processing systems*, 32, 2019.
- [9] Chandramouli Shama Sastry and Sageev Oore. Detecting out-of-distribution examples with gram matrices. In *International Conference on Machine Learning*, pages 8491–8501. PMLR, 2020.
- [10] Shiyu Liang, Yixuan Li, and R. Srikant. Enhancing the reliability of out-of-distribution image detection in neural networks. In *6th International Conference on Learning Representations, ICLR 2018, Vancouver, BC, Canada, April 30 - May 3, 2018, Conference Track Proceedings*. OpenReview.net, 2018.
- [11] Terrance DeVries and Graham W Taylor. Learning confidence for out-of-distribution detection in neural networks. *arXiv preprint arXiv:1802.04865*, 2018.
- [12] Yiyu Sun, Chuan Guo, and Yixuan Li. React: Out-of-distribution detection with rectified activations. *Advances in Neural Information Processing Systems*, 34, 2021.
- [13] In-Kwon Yeo and Richard A Johnson. A new family of power transformations to improve normality or symmetry. *Biometrika*, 87(4):954–959, 2000.
- [14] <https://github.com/FrejBerglind/xood>.
- [15] Kimin Lee, Kibok Lee, Honglak Lee, and Jinwoo Shin. A simple unified framework for detecting out-of-distribution samples and adversarial attacks. *Advances in neural information processing systems*, 31, 2018.
- [16] Chandramouli Shama Sastry and Sageev Oore. Detecting out-of-distribution examples with Gram matrices. In Hal Daumé III and Aarti Singh, editors, *Proceedings of the 37th International Conference on Machine Learning*, volume 119 of *Proceedings of Machine Learning Research*, pages 8491–8501. PMLR, 13–18 Jul 2020.

- [17] Sina Mohseni, Arash Vahdat, and Jay Yadawa. Shifting transformation learning for out-of-distribution detection, 2021.
- [18] Dan Hendrycks, Mantas Mazeika, and Thomas G. Dietterich. Deep anomaly detection with outlier exposure. In *7th International Conference on Learning Representations, ICLR 2019, New Orleans, LA, USA, May 6-9, 2019*. OpenReview.net, 2019.
- [19] Izhak Golan and Ran El-Yaniv. Deep anomaly detection using geometric transformations. *Advances in neural information processing systems*, 31, 2018.
- [20] Vikash Sehwal, Mung Chiang, and Prateek Mittal. Ssd: A unified framework for self-supervised outlier detection. *arXiv preprint arXiv:2103.12051*, 2021.
- [21] Jihoon Tack, Sangwoo Mo, Jongheon Jeong, and Jinwoo Shin. Csi: Novelty detection via contrastive learning on distributionally shifted instances. *Advances in neural information processing systems*, 33:11839–11852, 2020.
- [22] Weitang Liu, Xiaoyun Wang, John Owens, and Yixuan Li. Energy-based out-of-distribution detection. *Advances in Neural Information Processing Systems*, 33:21464–21475, 2020.
- [23] Jie Ren, Peter J Liu, Emily Fertig, Jasper Snoek, Ryan Poplin, Mark Depristo, Joshua Dillon, and Balaji Lakshminarayanan. Likelihood ratios for out-of-distribution detection. *Advances in Neural Information Processing Systems*, 32, 2019.
- [24] Apoorv Vyas, Nataraj Jammalamadaka, Xia Zhu, Dipankar Das, Bharat Kaul, and Theodore L Willke. Out-of-distribution detection using an ensemble of self supervised leave-out classifiers. In *Proceedings of the European Conference on Computer Vision (ECCV)*, pages 550–564, 2018.
- [25] Qing Yu and Kiyoharu Aizawa. Unsupervised out-of-distribution detection by maximum classifier discrepancy. In *Proceedings of the IEEE/CVF International Conference on Computer Vision*, pages 9518–9526, 2019.
- [26] Ziqian Lin, Sreya Dutta Roy, and Yixuan Li. Mood: Multi-level out-of-distribution detection. In *Proceedings of the IEEE/CVF Conference on Computer Vision and Pattern Recognition*, pages 15313–15323, 2021.
- [27] Sina Mohseni, Mandar Pitale, JBS Yadawa, and Zhangyang Wang. Self-supervised learning for generalizable out-of-distribution detection. In *Proceedings of the AAAI Conference on Artificial Intelligence*, volume 34, pages 5216–5223, 2020.
- [28] Rui Huang and Yixuan Li. Mos: Towards scaling out-of-distribution detection for large semantic space. In *Proceedings of the IEEE/CVF Conference on Computer Vision and Pattern Recognition*, pages 8710–8719, 2021.
- [29] Ananya Kumar, Aditi Raghunathan, Tengyu Ma, and Percy Liang. Calibrated ensembles: A simple way to mitigate id-ood accuracy tradeoffs. In *NeurIPS 2021 Workshop on Distribution Shifts: Connecting Methods and Applications*, 2021.
- [30] Dan Hendrycks, Steven Basart, Mantas Mazeika, Mohammadreza Mostajabi, Jacob Steinhardt, and Dawn Song. Scaling out-of-distribution detection for real-world settings. *arXiv preprint arXiv:1911.11132*, 2019.
- [31] Fahim Tajwar, Ananya Kumar, Sang Michael Xie, and Percy Liang. No true state-of-the-art? ood detection methods are inconsistent across datasets. *arXiv preprint arXiv:2109.05554*, 2021.

A: Additional Experiments

Table 5: Baseline/Energy/React/XOOD-L/XOOD-M.

			TNR (95% TPR)	Detection Acc.	AUROC
imagenet	resnet18	Uniform	2.5/ 100./100./100./100.	86.9/99.1/99.7/ 100./99.9	86.9/99.7/99.9/ 100./100.
		Gaussian	0.0/80.4/72.1/ 100./100.	76.0/95.3/94.4/ 100./99.9	65.1/96.2/95.8/ 100./100.
		Places	23.9/34.8/ 57.2/37.1/34.2	70.7/75.9/ 82.3/76.7/70.7	78.0/83.6/ 89.7/84.4/77.1
		SUN	26.4/40.0/ 65.5/46.9/48.6	71.6/78.4/ 85.3/79.9/77.9	78.9/86.1/ 92.7/88.0/85.2
		iNaturalist	41.6/43.2/ 69.9/60.9/38.9	78.9/82.5/ 87.4/84.8/74.4	87.0/89.8/ 94.6/92.8/82.0
		DTD	28.6/46.7/60.8/56.9/ 61.8	71.3/79.1/ 83.6/81.4/81.8	78.4/86.3/ 92.4/88.9/89.5
	resnet34	Uniform	86.4/ 100./99.6/100./100.	94.6/98.1/97.3/ 100./100.	97.2/98.7/98.4/ 100./100.
		Gaussian	48.6/ 0.0/ 0.0/ 100./100.	92.5/89.8/89.1/ 100./100.	94.3/85.9/85.2/ 100./100.
		Places	26.1/37.2/ 64.1/38.6/34.2	71.4/77.0/ 84.2/77.8/69.8	79.2/84.6/ 91.4/85.6/75.9
		SUN	27.6/42.6/ 73.6/48.4/48.1	72.3/79.2/ 87.5/81.0/76.9	79.8/86.6/ 94.0/88.6/83.8
		iNaturalist	40.5/46.0/ 75.9/65.1/40.2	78.3/82.2/ 88.8/86.1/74.1	86.6/89.7/ 95.7/93.7/81.5
		DTD	29.9/44.9/55.3/61.5/ 70.5	71.7/79.3/83.5/83.7/ 85.1	79.1/86.5/91.2/91.0/ 92.4
resnet50	Uniform	3.6/ 100./100./100./100.	89.7/98.3/99.6/ 100./100.	89.8/98.9/99.8/ 100./100.	
	Gaussian	0.0/ 0.0/ 0.0/ 100./100.	69.7/81.6/87.6/ 100./100.	53.2/75.5/85.8/ 100./100.	
	Places	28.0/34.8/ 66.6/43.5/32.0	72.8/76.9/ 85.0/79.6/69.9	80.6/84.2/ 92.0/88.7/75.9	
	SUN	31.0/41.9/ 76.0/54.4/47.8	74.0/79.4/ 87.9/82.7/77.6	81.7/86.8/ 94.4/90.4/84.8	
	iNaturalist	46.8/46.3/ 80.5/71.2/44.8	79.9/83.9/ 90.0/88.3/76.9	88.4/90.7/ 96.4/95.1/84.6	
	DTD	33.5/47.9/54.3/64.8/ 71.0	73.0/79.7/82.8/84.1/ 85.4	80.4/86.8/90.5/91.3/ 92.9	
resnet101	Uniform	27.1/96.7/ 100./100./100.	87.3/96.5/99.3/ 100./100.	90.8/97.2/99.6/ 100./100.	
	Gaussian	0.0/ 0.0/ 100./100./100.	79.0/88.0/98.3/ 100./100.	70.6/83.9/98.2/ 100./100.	
	Places	28.8/39.4/ 63.7/42.7/26.7	72.9/78.2/ 84.2/79.7/71.2	80.6/85.5/ 91.3/87.2/77.0	
	SUN	32.1/46.8/ 73.4/51.0/41.3	73.9/80.6/ 87.2/82.6/78.3	81.4/87.7/ 94.0/89.9/85.2	
	iNaturalist	42.9/41.6/ 79.1/61.9/32.5	77.4/81.1/ 89.5/86.3/75.7	86.2/88.3/ 96.1/93.4/82.8	
	DTD	37.4/52.6/59.6/67.5/ 68.6	73.4/80.8/83.5/85.4/ 87.2	81.5/87.9/91.4/92.4/ 94.0	
cifar10	resnet	Uniform	72.7/82.0/90.2/ 100./100.	93.6/94.2/94.6/ 100./100.	96.1/96.2/96.8/ 100./100.
		Gaussian	90.8/98.8/98.1/ 100./100.	95.7/97.0/96.6/ 100./100.	97.5/98.0/98.2/ 100./100.
		TinyImageNet (Crop)	46.9/62.1/65.1/98.0/ 99.1	85.5/86.5/86.5/96.7/ 98.0	91.6/93.1/92.6/99.9/ 99.8
		TinyImageNet (Resize)	45.1/59.5/63.9/97.9/ 99.5	85.1/85.8/86.3/96.9/ 98.8	91.1/92.5/92.4/99.6/ 99.9
		LSUN (Crop)	49.1/65.7/62.5/ 97.0/94.6	86.4/87.5/85.1/ 96.0/94.8	92.0/93.9/90.9/ 99.4/99.0
		LSUN (Resize)	46.3/62.9/69.4/99.1/ 99.9	85.5/86.7/88.2/97.8/ 99.2	91.3/92.9/94.4/99.8/ 100.
	densenet	iSUN	45.6/62.0/68.0/99.1/ 99.7	85.2/86.3/87.9/97.8/ 98.8	91.2/92.8/94.2/99.8/ 99.9
		SVHN	33.3/47.9/37.9/96.4/ 98.4	85.4/85.5/77.5/96.1/ 97.6	90.1/91.3/83.3/99.3/ 99.7
		Cifar100	34.2/ 44.0/44.0/43.6/32.0	80.5/80.7/78.7/ 81.7/73.7	86.6/87.3/84.4/88.8/ 80.1
		Uniform	78.0/96.7/ 100./100./100.	94.8/96.3/98.1/ 100./100.	96.7/97.4/99.2/ 100./100.
		Gaussian	89.3/ 100./100./100./100.	95.4/97.9/98.4/ 100./100.	97.7/98.9/99.5/ 100./100.
		TinyImageNet (Crop)	57.4/84.1/68.6/ 98.6/97.8	88.2/91.6/87.6/ 97.7/96.6	94.0/97.1/94.1/99.7/ 99.5
svhn	resnet	TinyImageNet (Resize)	60.1/86.2/68.7/99.1/ 99.2	88.8/92.3/87.3/ 98.2/97.8	94.3/97.5/94.0/ 99.8/99.8
		LSUN (Crop)	52.4/76.1/66.4/ 96.9/91.7	87.2/89.8/88.4/ 96.1/93.6	93.2/96.0/94.4/ 99.3/98.4
		LSUN (Resize)	67.3/92.3/83.1/99.4/ 99.7	90.5/93.9/91.4/98.5/ 98.6	95.6/98.4/96.9/ 99.9/99.9
		iSUN	63.8/89.3/78.4/ 99.5/99.4	89.5/93.1/90.0/ 98.5/98.1	95.0/98.0/96.1/ 99.9/99.8
		SVHN	40.9/52.9/65.3/96.5/ 97.2	83.4/83.5/88.1/96.2/ 96.7	90.1/91.1/93.8/99.2/ 99.3
		Cifar100	41.7/ 55.3/49.3/47.6/19.9	83.2/ 83.6/82.2/78.6/64.8	89.6/ 90.7/89.2/87.0/70.7
	densenet	Uniform	85.9/86.7/71.9/ 100./100.	93.0/92.5/84.7/99.5/ 99.7	96.1/95.6/89.4/ 100./100.
		Gaussian	86.1/87.3/75.2/ 100./100.	93.0/92.7/86.1/99.7/ 99.9	96.3/96.0/90.5/ 100./100.
		TinyImageNet (Crop)	81.3/83.0/74.4/ 99.7/99.7	91.1/90.7/85.5/ 98.7/98.3	94.2/93.8/88.7/99.9/ 99.8
		TinyImageNet (Resize)	79.8/81.5/74.1/99.7/ 99.8	90.6/90.1/85.2/98.4/ 98.6	93.6/93.0/88.9/ 99.9/99.8
		LSUN (Crop)	77.2/79.0/71.5/ 99.2/98.6	89.9/89.4/84.0/ 97.7/97.0	92.9/92.5/86.2/ 99.7/99.5
		LSUN (Resize)	75.5/77.2/67.2/99.5/ 99.9	89.1/88.3/82.0/98.3/ 98.9	91.6/90.7/84.9/ 99.9/99.9
cifar100	resnet	iSUN	78.1/79.8/69.0/99.8/ 99.9	89.9/89.4/82.7/98.7/ 98.9	92.3/91.5/85.6/ 99.9/99.9
		Cifar100	77.7/78.9/74.0/ 97.8/95.5	89.5/88.9/85.2/ 96.4/95.5	92.4/91.5/89.1/ 99.3/98.9
		Uniform	66.3/64.0/37.9/ 100./100.	87.7/83.6/79.0/ 100./100.	93.2/90.1/87.2/ 100./100.
		Gaussian	88.2/90.8/55.9/ 100./100.	93.5/93.2/84.1/ 100./100.	97.4/97.8/91.2/ 100./100.
		TinyImageNet (Crop)	79.1/77.1/72.4/ 100./99.9	89.9/87.4/86.6/ 99.4/99.3	94.7/92.8/93.2/ 100./100.
		TinyImageNet (Resize)	80.1/78.7/73.1/ 100./100.	90.3/88.1/87.0/99.5/ 99.6	94.9/93.4/93.5/ 99.1/100.
	densenet	LSUN (Crop)	74.0/67.8/71.6/ 99.7/99.2	88.1/83.2/85.5/ 98.7/97.8	93.0/88.5/92.1/ 99.9/99.8
		LSUN (Resize)	77.4/76.8/70.6/ 100./100.	89.3/87.1/85.4/ 99.8/99.8	94.2/92.6/92.3/ 100./100.
		iSUN	78.7/78.2/70.2/ 100./100.	89.8/87.6/85.8/99.7/ 99.8	94.5/92.9/92.6/ 100./100.
		Cifar100	68.5/64.6/74.8/ 98.1/97.9	86.6/83.0/87.3/ 96.8/96.7	91.4/88.2/93.9/ 99.5/99.4
		Uniform	12.1/ 1.6/ 1.3/ 100./100.	81.5/84.7/80.6/ 100./100.	85.2/86.5/81.6/ 100./100.
		Gaussian	0.0/ 0.0/ 0.0/ 100./100.	60.7/60.8/81.7/ 100./100.	45.1/46.1/76.6/ 100./100.
cifar100	resnet	TinyImageNet (Crop)	25.0/27.1/28.5/90.8/ 95.0	72.6/74.4/71.2/93.2/ 95.0	79.7/81.6/78.9/98.4/ 98.9
		TinyImageNet (Resize)	21.3/25.3/25.6/89.4/ 97.9	71.0/73.0/68.6/92.6/ 96.7	77.2/80.1/76.2/98.1/ 99.5
		LSUN (Crop)	19.2/18.0/28.0/ 85.3/76.2	69.6/69.2/77.7/ 91.4/88.2	75.6/75.1/84.3/97.5/ 95.3
		LSUN (Resize)	19.4/23.3/23.0/90.2/ 98.5	70.0/71.9/68.5/92.9/ 97.4	75.7/78.5/75.5/98.3/ 99.6
		iSUN	17.7/20.9/21.5/89.6/ 97.0	70.3/72.1/68.5/92.8/ 96.2	75.8/78.2/75.3/98.3/ 99.3
		SVHN	21.3/18.8/26.3/87.2/ 92.1	73.4/73.5/77.3/91.5/ 93.6	79.5/79.5/84.2/97.6/ 98.2
	densenet	Uniform	0.0/ 0.0/ 0.0/ 100./100.	64.2/66.7/76.1/ 100./100.	43.3/50.3/74.0/ 100./100.
		Gaussian	0.0/ 0.0/ 0.0/ 100./100.	58.9/53.0/69.8/ 100./100.	30.8/15.6/58.2/ 100./100.
		TinyImageNet (Crop)	23.5/39.3/65.1/ 95.4/89.2	68.8/76.9/86.4/ 95.2/92.7	75.9/84.8/93.7/ 99.1/97.5
		TinyImageNet (Resize)	16.6/22.8/64.4/95.7/ 96.1	65.9/71.4/86.8/95.4/ 95.6	71.5/78.2/93.8/ 99.2/98.9
		LSUN (Crop)	27.5/51.9/43.8/ 84.9/68.4	72.5/82.2/79.0/ 91.3/85.0	79.8/90.1/87.2/ 97.4/92.6
		LSUN (Resize)	15.8/22.0/72.8/94.3/ 97.9	65.0/72.4/88.8/94.8/ 96.7	70.6/79.5/95.3/99.0/ 99.3
cifar100	resnet	iSUN	14.2/18.2/68.4/94.0/ 96.3	64.0/70.5/86.9/94.6/ 95.7	69.5/77.2/93.9/98.9/ 99.0
		SVHN	25.2/33.2/33.1/ 88.8/87.9	75.5/80.5/79.5/ 92.3/91.9	82.4/87.7/86.9/ 97.7/97.1

B: Feature Selection

In this section, we report experimentation with a number of different features: only using the minimum or maximum, the percentage of positive values (positivity); the sum; L_p -norms; L_p -norms of $\text{ReLU}(x)$ and $\text{ReLU}(-x)$ (Split L_p). As one can see in Tables 6 and 7, neither replacing the extreme values by these features, nor adding these features while still using the extreme values improves the detection performance.

	cifar10		densenet		svhn		densenet		cifar100		densenet	
	resnet				resnet				resnet			
	XOOD-M	XOOD-L	XOOD-M	XOOD-L	XOOD-M	XOOD-L	XOOD-M	XOOD-L	XOOD-M	XOOD-L	XOOD-M	XOOD-L
Min & Max	99.7	99.47	99.4	99.55	99.77	99.85	99.94	99.97	98.42	97.86	97.3	98.29
Min	99.63	99.4	99.23	99.41	99.43	99.77	99.87	99.93	98.17	98.04	96.63	96.84
Max	99.59	99.32	99.43	99.54	99.6	99.69	99.91	99.97	97.4	97.13	97.37	97.48
Positivity	97.86	98.76	95.56	98.22	99.43	99.82	99.45	99.81	89.76	90.47	91.38	92.06
Sum	97.67	98.92	96.06	97.1	99.54	99.81	99.64	99.75	92.2	96.41	92.32	92.82
L1	98.15	98.75	98.11	98.2	98.87	99.53	99.69	99.74	93.55	95.77	92.22	94.18
L2	98.5	98.78	98.57	98.68	98.98	99.51	99.78	99.82	93.71	96.01	93.19	94.78
L3	98.83	98.9	98.83	98.99	99.16	99.54	99.8	99.87	94.74	95.96	94.01	95.37
Split L1	98.59	98.96	98.2	98.19	99.69	99.78	99.82	99.88	95.36	96.23	93.03	93.13
Split L2	98.94	99.08	98.61	98.89	99.61	99.72	99.86	99.89	95.94	97.36	93.6	94.74
Split L3	99.23	99.18	98.92	99.24	99.69	99.82	99.88	99.92	96.8	97.5	94.33	95.66

Table 6: AUROC-score when replacing the extreme values with other features which have linear computational complexity.

	cifar10		densenet		svhn		densenet		cifar100		densenet	
	resnet				resnet				resnet			
	XOOD-M	XOOD-L	XOOD-M	XOOD-L	XOOD-M	XOOD-L	XOOD-M	XOOD-L	XOOD-M	XOOD-L	XOOD-M	XOOD-L
Min & Max	99.7	99.46	99.4	99.5	99.77	99.85	99.94	99.97	98.42	97.8	97.3	98.18
Positivity	99.68	99.54	99.27	99.34	99.88	99.92	99.95	99.98	98.14	97.21	97.0	97.52
Sum	99.64	99.5	99.28	99.19	99.9	99.93	99.94	99.96	98.22	97.66	96.85	97.45
L1	99.62	99.43	99.33	99.38	99.79	99.87	99.93	99.92	98.3	97.5	96.63	97.74
L2	99.63	99.42	99.37	99.39	99.79	99.78	99.94	99.92	98.18	97.61	96.69	97.86
L3	99.63	99.43	99.39	99.39	99.8	99.78	99.94	99.93	98.18	97.58	96.76	97.97
Split L1	99.57	99.43	99.26	99.17	99.9	99.91	99.93	99.95	98.21	97.5	96.33	97.11
Split L2	99.59	99.41	99.29	99.22	99.86	99.87	99.94	99.94	98.13	97.82	96.28	97.51
Split L3	99.62	99.44	99.33	99.25	99.87	99.87	99.93	99.94	98.21	97.85	96.36	97.74

Table 7: AUROC-score when extracting additional extreme values before each activation layer.

C: Extreme Value Distributions

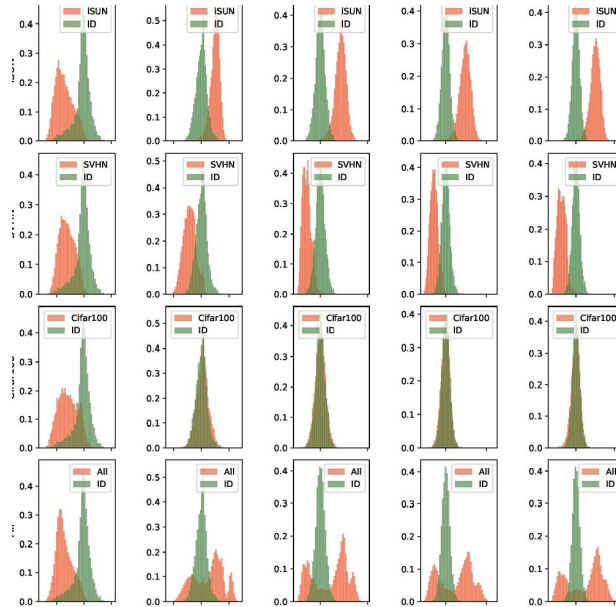


Figure 4: Distribution of maximum values before an activation layer inside ResNet34. Green represents CIFAR-10 (In-distribution (ID)) and Orange represents OOD. Note how in-distribution data lies in a single mode, while out-of-distribution data can be on either side.

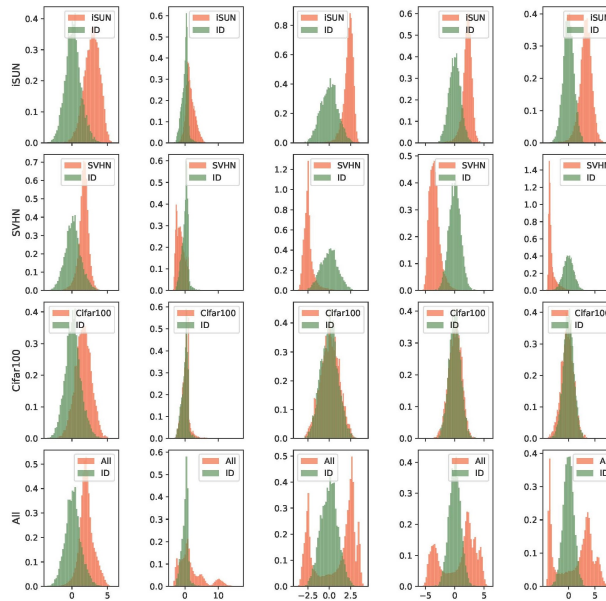


Figure 5: Distribution of minimum values before an activation layer inside ResNet34. Green represents CIFAR-10 (In-distribution (ID)) and Orange represents OOD. Note how in-distribution data lies in a single mode, while out-of-distribution data can be on either side.

D: False Positive Rate

To summarize the performance of the various methods in Table 1 and 2, we computed the mean FPR (95% TPR) for each OOD detection task, except the CIFAR-10–CIFAR-100 and CIFAR-100–CIFAR-10 in-distribution-OOD combinations, given their overlap. These averages are shown in Table 8. Note that XOOD-L and XOOD-M have the best average scores for both DenseNet and ResNet. For DenseNet, XOOD-L reduced the FPR by 48% compared to the best other method (Gram), and for ResNet34 XOOD-M reduced the FPR by 51% compared to the best other method (Gram).

	Baseline	ODIN	Mahalanobis	Gram	XOOD-L	XOOD-M
ResNet34	55.7	37.6	8.6	7.1	5.2	3.5
DenseNet	51.8	28.4	15.2	6.9	3.6	5.1

Table 8: Average FPR at 95% TPR. Lower score is better.